Influence of the mass of energetic material and stand-off distance on the performance of perforator charges

Influence of the mass of energetic material and stand-off distance on the performance of perforator charges

A Abd Elhady[1,3], A M Riad[2] and M A Shaker[2] and T A Elshenawy[1]

[1] Technical Research Centre, Cairo, Egypt.
[2] Weapons and Amm. Dept., Mechanical Engineering Branch, Military Technical College, Kobri El-Kobba, Cairo, Egypt.

[3] Email: a7md3abhady@gmail.com.

Abstract. In this paper, the influence of the mass of Energetic Material (EM) and the relevant stand-off distance on the perforator charge performance has been investigated experimentally and numerically. An experimental program has been conducted, in which perforator charges have been constructed using different masses of an EM; where the relevant stand-off distances for the perforator charges have been changed accordingly. The constructed perforator charges with 33 mm in diameters are statically exploded against 1006 steel target and the depth of jet penetration for each tested perforator charge has been measured. Moreover, Autodyn-2D hydrocode is fed with the data of the constructed perforator charges to simulate their jet formation and its penetration process into 1006 steel target. The hydrocode predicts the dependence of the resultant jet velocity and its penetration depth into 1006 steel target on the mass of EM and the relevant stand-off distance. This dependence has also been confirmed by the corresponding static test results of small diameters perforator charges. Results show that the measured penetration depth increases from 11.0 to 13.7cm into 1006 steel target when the mass of EM increases from 36 to 41g and the relevant standoff distance decreases from 25.6 to 22.6 mm then; the penetration depth decreases again due to the limited standoff distance maintained for the tested perforator charges.

Keywords. C10100 Copper; perforator charge, stand-off distance, and energetic materials.

1. Introduction

Perforator charges are Energetic Material (EM) equipment with very high penetration capability and have wide military and civil applications. The perforator charge consists of three main parts; they are liner, EM and metallic casing. The EM and liner are placed inside the casing. The EM is surrounded by the liner from the front and the casing from the back. With the detonation of EM, a spherical high-pressure wave is generated. This detonation wave propagates with a velocity of 7000 m/s and a pressure of $3x10^{10}$ Pa [1]. The liner material is collapsed under tremendous high pressure generated from the used EM, colliding with other collapsed liner elements to create a hypervelocity jet with a high liner strain rate as much as 10^4 to $10^7 s^{-1}$ [2]. The succeeded jet moves under this extremely high pressure with a tip velocity about 9 km/s. The resulting jet elongates due to the presence of a velocity gradient along its length and the stand-off distance between the charge base and the target surface. The formed jet is either totally consumed during target penetration or it breaks up into smaller fragments, after which the jet does not become effective anymore.

Apart from the target material types, the jet penetration into target material was mainly affected by the effective jet length, jet density and its tip velocity [3]. These parameters were significantly depended on the loaded mass of EM and the charge design. The stand-off distance was considered as a key parameter for effective penetration of jet [4]. If it was too large, the jet may particulate into small fragments with drift velocity and noticeable decreasing in penetration depth. Also, the short stand-off distance did not allow the proper formation of jet and thus it reduced the penetration potential of the perforator charge because the jet tip did not have the required velocity and the effective length of jet was not reached [5]. The stand-off distance was generally expressed in terms of the Charge Diameter (CD), which could be optimized at three to five times the CD [1], at which the penetration was maximum.

Various studies have been conducted to investigate the effect of stand-off distance, type of EM and the EM-to-liner mass ratio on the jet formation and its penetration capability of various targets. Held [6] used the results of three firings of 150 mm perforator charges at 6, 12 and 24 CD stand-off distances, respectively, against rolled homogeneous armour (RHA) targets to study the effect of stand-off distance on the penetration performance of perforator charge jets in terms of their cut-off velocities. The cut off velocity was determined from the stand off–cut off diagram, using the measured depths of penetration listed in table 1. He found that the cut-off velocity increases with the stand-off distance, which leads to decreasing the achieved penetration depths into RHA targets considering constant jet tip velocity at these stand-off distances.

Table 1. Results of the firing tests made by Held [6].

Stand-off, (CD)	Cut-off velocity, (km/s)	Penetration, (mm)
6	4.3	1097
12	5.26	1030
24	6.75	613

Dehestani et al. [7] investigated numerically the collapsing mechanism, jet formation and its penetration into metallic target using ABAQUS/Explicit code. They considered the strain rate dependency and thermal effect of jet material in their model. They compared the penetration depths into steel target for a group of tested perforator charges with the corresponding predictions; good agreement was generally obtained. They also investigated numerically the effect of standoff distances and liner thicknesses, respectively, on penetration depth. They concluded that: i) if the standoff distance is less than the allowed limit, the jet impacts the target before reaching its maximum length, and consequently it has a negative effect on the jet penetration depth, and ii) the decrease of liner thickness leads to the formation of a more elongated jet with a higher velocity, which in turn increases the jet penetration depth into target.

Tien et al. [8] developed a new method for predicting the optimum standoff distance of a perforator charge using Autodyn-2D hydrocode. The developed method was applied to PG-7V perforator charge. In their simulation, the optimum stand-off distance for the perforator charge was predicted for the formed continuous jet having a highest length before impacting the target. Their predicted optimum stand-off distance was consistent with that reported in the technical documentation of PG-7V warhead.

El-Sayed et al. [9] investigated the influence of liner thickness of perforator charges on their penetration performance experimentally and numerically. They conducted an experimental program in which they constructed perforator charges with liner thicknesses ranged from 0.8 to 1.2 mm. They tested these charges by exploding them statically against steel target. Moreover, Autodyn-2D hydrocode was used to simulate the penetration process of tested perforator charges with different liner thicknesses into steel target using two algorithms; they are jetting analyses and jet formation and penetration, respectively. Good agreement was generally obtained between the predicted penetration depth and the corresponding measurement. They also extended their numerical work by selecting the perforator charge that gave the maximum jet penetration into steel target to study the influence of other different perforator charge parameters on penetration performance. They found that the best perforator charge performance is associated with both the type of EM and the standoff distance, respectively.

Zaki et al. [10] performed ballistic tests for a group of perforator charges on RHA targets to provide data about their penetration performance. Their experimental data were compared with the corresponding numerical results obtained by Autodyn-2D hydrocode; good consistency was obtained between their measurements and the corresponding predictions of Autdyn-2D hydrocode. Then, they used their numerical model to investigate the effect of liner material and EM type on the lethality of perforator charges. They fed the model with the data of three types of liner materials and three types of energetic materials, respectively. The liner materials were copper, tantalum and aluminum whereas; the EM types were RDX, Comp B and HMX. They concluded that: i) the EM type HMX gives the highest velocity of the formed jet compared with the other two types of EM and ii) the jet formation from both copper and tantalum liners, respectively, is coherent while aluminum liner results in a particulated jet.

Because of the perforator charge height is limited; the increase in the mass of EM results in a decreasing in the stand-off distance. In the following, the influence of the mass of EM and the relevant standoff distance on the penetration performance of perforator charges has been investigated experimentally and numerically. The perforator charges have been constructed using different masses of EM and consequently different stand-off distances. Then, their ballistic tests have been performed by exploding them statically against 1006 steel target. In addition, Autodyn-2D hydrocode is fed with the data of the tested perforator charges to predict the influence of the studied parameters on the perforator charge performance. Samples of the obtained results due to the impact of these two parameters on achieved penetration depth into steel target will be presented and discussed.

2. Experimental work

An experimental program has been conducted to construct small size perforator charges with different EM mass to measure their penetration potential into steel target. In the following, the manufacturing techniques for both the liner and the EM are presented together with the charge assembly and setup of field test.

2.1. The liner

The manufacturing process used for the production of copper perforator charges was the flow forming process, in which an annealed C10100 copper blank with purity of 99.99% was plastically deformed by a roller tool over a mandrel at room temperature to achieve the desired shape as shown in figure 1. This plastic deformation caused the cone wall to be thinner than the original plate and also leaded to work hardening. Excess flash material on the rim of the cone was machined off. The cone was then annealed at controlled temperature to remove work hardening by recrystallization of the grain structure and to achieve fully equi-axed grains with sizes less than 30 μm [11]. The manufactured trumpet copper liners had base diameters of 33 mm and uniform wall thicknesses of 1.1 mm.

2.2. The charge assembly and the static firing

The EM amount used to fill the steel body of each of the perforator charges was divided into four equal masses; each mass was pressed inside the steel body using uniaxial press with capacity of 200 MPa. The pressing process was performed slowly to exit the present air without affecting the uniformity and homogeneity of the detonation wave when the charge was detonated. The final stage of pressing was performed using a mandrel having identical shape to the outer surface of the liner material. After loading and pressing the four stages, the liner was then inserted gently inside the formed EM cavity. Then, X-ray photographs were taken for the assembled charges; cf. figure 2, to ensure there was neither air voids nor cracks inside EM or at the copper liner-EM interface.

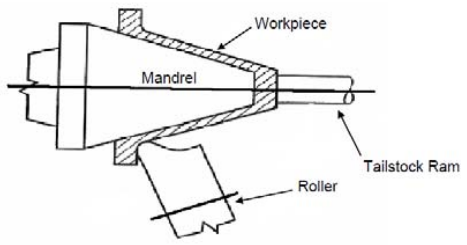

Figure 1. Flow forming process [11].

Figure 2. A sample of the X-ray photograph of a perforator charge.

Each filled perforator charge with a specified mass of EM was attached to the upper surface of laminated 1006 steel target and exploded statically using an electric detonator, see figure 3. Then, the laminated layers were cut down vertically to measure the penetration depth and the crater profile associated with each tested perforator charge as shown in figure 4.

3. Numerical simulation

For each tested perforator charge with a specific mass of EM, Autodyn-2D hydrocode simulates the jet formation and its penetration into steel target. Input data to the hydrocode are that of the tested perforator charges. In the following, the different schemes of Autodyn-2D hydrocode and material models of the perforator charge elements that used in the current numerical work are introduced.

Figure 3. Perforator charge attached to steel target.

Figure 4. Cutting of laminated layers of 1006 steel target after tests.

3.1. Algorithms of Autodyn-2D hydrocode

3.1.1. Jetting analysis algorithm. The jet and slug velocities and their masses were predicted using such an algorithm that based on the unsteady state PER theory [12]. This algorithm treated the liner thickness of 1.1mm as a thin shell and it specified that the apex point as fixed by a boundary in order to prevent its motion [13]. The contact polygon surface defined the interaction surface between the shell liner and EM. The outputs of such an algorithm included the collapse, flow and jet velocities of liner elements, liner collapse and deflection angles, as well as the kinetic energy and momentum of the formed jet.

3.1.2. *The jet formation algorithm*. It was simulated using Euler method based on continuum mechanics to obtain the jet profiles at different time stages. The EM, charge casing, and liner materials were filled into the global Euler multi-material parts [13]. In addition, the interaction between the formed jet and the target was not taken into account. The detonation wave swept the collapsed liner to generate the jet and the slug when the EM was detonated. The formed jet and slug flew over the fixed size Euler meshes with a non-uniform velocity distribution in the direction of the target. The output of such an algorithm would be the input for next algorithm.

3.1.3. *The jet penetration algorithm*. It was used to simulate its interaction (penetration) with the target. The jet obtained from the jet formation Euler solver was remapped to Lagrange moving grids and struck the target. A mesh discard option or erosion strain was applied to the jet and the target materials in order to overcome the mesh distortion issue in the Lagrange solver. The erosion strain was not a real phenomenon, but rather a numerical procedure for preventing mesh distortions [14]. Erosion strains of 0.5 and 3 were used for target and copper liner materials, respectively.

3.2. Material models:

In the following, the material models and parameters that have been used in Autodyn-2D hydrocode for simulating of jet formation and penetration are briefly discussed for EM, liner, casing and target materials, respectively. Initial setup for the discussed parameters including the EM head height (H.H) and S.O.D (stand-off distance) is shown in figure 5. In addition, the values of H.H, S.O.D and the mass of EM for each trial designation are listed in table 2.

3.2.1. The energetic material. The type of EM used for filling the meshes inside the perforator charge was HMX. The equation of state (EOS) for this EM is "Jones-Wilkins-Lee" (JWL) equation [15], i.e.,

$$p = A\left(1 - \frac{\omega}{r_1 v}\right)e^{-r_1 v} + B\left(1 - \frac{\omega}{r_2 v}\right)e^{-r_2 v} + \frac{\omega E}{v} \quad (1)$$

where *p* is the pressure; v (=1/ρ) is the specific volume where ρ is the current material density; E is the specific internal energy per unit mass; A, B, r_1, r_2 and ω are material constants that are determined and listed in table 3 for EM type HMX.

3.2.2. Liner material. The material used for filling the meshes of liner elements was copper. The equation of state for the used material was shock and the strength model was none due to the very high shock pressure compared with strength of liner material. The Mie-Gruneisen equation of state based on the

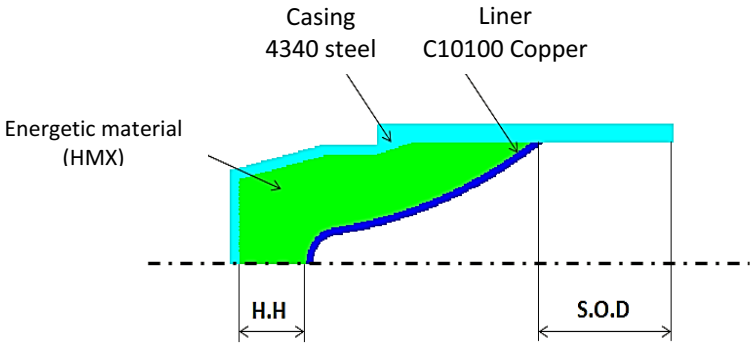

Figure 5. Perforator charge with trumpet liner thickness of 1.1 mm.

Table 2. Span of the studied parameters.

(a)

Trial design.	Distance, (H.H) (mm)	S.O.D. (mm)	Mass of EM (g)
A	4.58	26.6	34.57
B	5.58	25.6	36.20
C	6.58	24.6	37.82
D	7.58	23.6	39.44
E	8.58	22.6	41.07
F	9.58	21.6	42.69
G	10.58	20.6	44.31
H	11.58	19.6	46.08

(b)

Trial design.	Distance (H.H) (mm)	S.O.D. (mm)	Mass of EM (g)
I	12.58	18.6	47.56
J	13.58	17.6	49.18
K	14.58	16.6	50.81
L	15.58	15.6	52.43
M	17.58	13.6	55.67
N	19.58	11.6	58.92
O	21.58	9.6	62.16
P	23.58	7.6	65.41

Table 3. The JWL constants and detonation characteristics of the used EM type.

(a)

Parameter	Value
Density (g/cm^3)	1.83
Parameter A (MPa)	8.261×10^5
Parameter B (MPa)	1.724×10^4
Parameter r_1	4.55
Parameter r_2	1.32

(b)

Parameter	Value
C-J Detonation velocity (m/s)	8800
C-J Energy per unit volume (kJ/m^3)	1.02×10^7
C-J Pressure (MPa)	3.7×10^4
Parameter ω	0.38

shock Hugoniot was used to represent the equation of state for liner material. This equation is expressed by [13]:

$$p = p_H + \Gamma\rho(E - E_H) \quad (2)$$

where Γ is the Gruneisen gamma coefficient and is equal to [B_o / (1+μ)]; B_o is a constant and μ is the compressibility, P_H and E_H are the Hugoniot pressure and energy, respectively, given by:

$$p_H = \frac{\rho_o c_o^2 \mu(1+\mu)}{[1-(s-1)\mu]^2} \tag{3}$$

and

$$E_H = \frac{1}{2}\frac{p_H}{\rho_o}\left(\frac{\mu}{\mu+1}\right) \tag{4}$$

where c_o is the sound velocity in the material, and s is constant giving the slope of shock velocity-particle velocity relationship. More detailed information about the used equation of state is reported in Ref. [13]. Autodyn-2D hydrocode was fed with the data listed in table 4 for the copper liner material with wall thickness of 1.1 mm and mass of 22.6 g. The constants of the previous equations were taken from the material library of the hydrocode.

3.2.3. Charge case material. The material used for the charge case was 4340 steel with shock EOS, which has been described previously for the copper liner material, while its strength model was Johnson-Cook in order to model the strength behavior of materials subjected to large strains, high strain-rates and high temperatures [16]; i.e.

$$Y = \left(A + B\varepsilon_p^n\right)\left(1 + C\log\dot{\varepsilon}_p\right)\left(1 - T_H^m\right) \tag{5}$$

where Y is the dynamic flow stress; ε_p is the effective plastic strain, $\dot{\varepsilon}_p$ is the normalized effective plastic strain-rate and $T_H^m = (T - T_{room})/(T_{melt} - T_{room})$ is the homologous temperature; A, B, C, n and m are the material constants; T_{melt} is the melting temperature. The constants in these expressions were determined by means of material tests over a range of temperatures and strain-rates. The input data to the hydrocode for the charge case material are listed in table 4.

Table 4. Input data to the hydrocode for steel and copper materials, respectively [17].

(a)

Parameter	4340 Steel	OFHC Copper
EOS	Shock	Shock
Ref. density, ρ_o (g/cm^3)	7.83	8.90
A (MPa)	792	-
B (MPa)	510	-
n (none)	0.26	-
C (none)	0.014	-

(b)

Parameter	4340 Steel	OFHC Copper
m (none)	1.03	-
Gamma Coeff., Γ	1.93	2.02
C_o, (m/s)	4569	3940
S, (none)	1.4	1.489
T_r (K)	300	300
(K)	2380	1356

3.2.4. Target material. The used target material was 1006 steel with a density of 7.896 g/cm^3 and shock EOS of with Gruneisen coefficient of 2.17, parameter C = 4569 m/s and S = 1.49. The strength model used with the Steel target was Johnson-Cook model; the shear modulus of the used target material was 8.18 x 10^4 MPa whereas; its yield strength was 350 MPa.

4. Results and discussion

4.1 Mesh sensitivity results

It is known that the mesh size affects the accuracy of the numerical results obtained. Using a fine mesh gives accurate results, but it takes much more time than if a coarse mesh is used. The mesh sensitivity study was performed for the jetting analysis, jet formation and jet penetration algorithms. For space limitation, the main procedures for determining the mesh sizes of each perforator charge element during running of each algorithm are reported in Ref. [18].

4.2 Jetting analysis results

The jetting analysis algorithm was used to determine the velocity and mass of each formed jet element in addition to the values of jet mass, kinetic energy and its momentum for each studied design. The values of some of these parameters are listed in table 5. Based on momentum conservation principle, the tip velocity of jet V_{tip} is determined by [1]:

$$V_{tip} = \frac{\int_0^{X_{tip}} V_j\left(dm_j/dX\right)dX}{\int_o^{X_{tip}}\left(dm_j/dX\right)dX}\ , \tag{6}$$

where X is the position of liner element. Figure 6 plots the predicted course of jet velocity for the studied perforator charge with mass of EM of 39.44g and the calculated tip velocity of jet V_{tip} using equation 6.

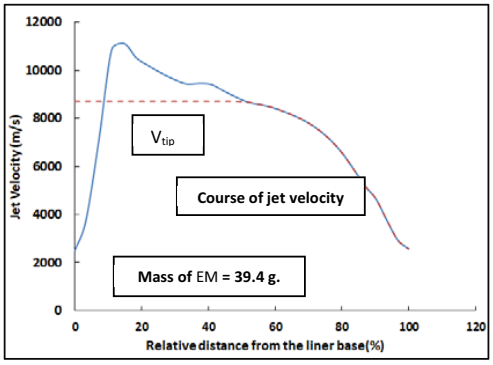

Figure 6. Predicted course of jet velocity for the perforator charge with EM of 39.44g and the calculated V_{tip} using equation 6.

The calculated masses of EM for the perforator charge trials are ranged from 34.57 to 65.41g as listed in table 2. The purpose of the data summarized in table 5 is to investigate the effect of both the mass of EM and the relevant stand-off distance of the studied perforator charges on their penetration performance into steel target to identify the best design that may be selected according to jet energy characteristics.

Table 5. Jetting analysis results for studied trials of perforator charges.

(a)

Trial design.	Jet mass, (g)	(Jet/liner) mass ratio, (%)	Jet tip velocity, V_{tip} (m/s)	Kinetic energy of jet (kJ)
A	3.57	15.80	8637.8	51.26
B	3.59	15.88	8639.6	52.32
C	3.64	16.11	8667.8	53.32
D	3.66	16.19	8698.9	54.31
E	3.69	16.33	8754.5	55.27
F	3.71	16.42	8795.9	56.18
G	3.72	16.46	8842.4	57.07
H	3.76	16.64	8899.6	57.80

(b)

Trial design.	Jet mass, (g)	(Jet/liner) mass ratio, (%)	Jet tip velocity, V_{tip} (m/s)	Kinetic energy of jet (kJ)
I	3.79	16.77	8964.1	58.76
J	3.81	16.86	9029.5	59.55
K	3.82	16.90	9075.7	60.30
L	3.84	16.99	9146.8	61.04
M	3.89	17.21	9246.5	62.40
N	3.92	17.35	9366.2	63.58
O	3.95	17.48	9468.2	64.59
P	4.01	17.74	9565.4	65.41

In general, the increase in the mass of EM enhances the EM/liner mass ratio; which in turn increases the jet collapse, flow, stagnation and tip velocities, accordingly. In addition, it also increases the jet mass and its ratio to the liner mass in percent. The obtained data from the jetting analysis algorithm must be treated carefully when using them for further calculations; e.g. the determination of the jet penetration depth into steel target using the analytical formulae developed by Allison and Vitalli [19].

Figure 7 shows that the predicted tip velocity increases with the EM mass of perforator charges designated from A to P. This may be attributed to the increase in the (EM/liner) mass ratio, which in turn

increases the liner collapse velocity. This collapse velocity is directly proportional to the stagnation, flow and tip velocities of jet, respectively, in accordance with unsteady PER theory [12]. The increase in the jet tip velocity when the mass of EM ranged from 33 to 39g is very slow; after that the increase in the mass of EM causes a significant increase in the jet tip velocity. On the other hand, it has been concluded from table 5 that the kinetic energy of jet increases with jet mass and the mass of EM. The relation between jet kinetic energy and mass of EM can be well described by an exponential relation as shown in figure 8.

4.3. Jet formation results

The jet formation algorithm is run to predict the jet profile and its various parametric contours such as velocity, pressure, and temperature. In addition, jet velocity results are important for determining the virtual origin point using back projection method [20]. Figure 9 shows a sample of the velocity profile contour of the jet formed from the liner of perforator charge with EM mass of 42.6g just before assigning the stand-off distance.

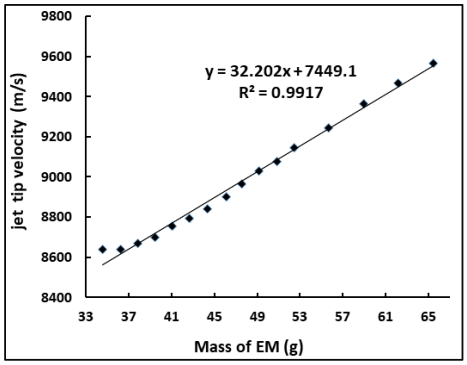

Figure 7. Predicted change of jet tip velocity V_{tip} with mass of EM for different perforator charges.

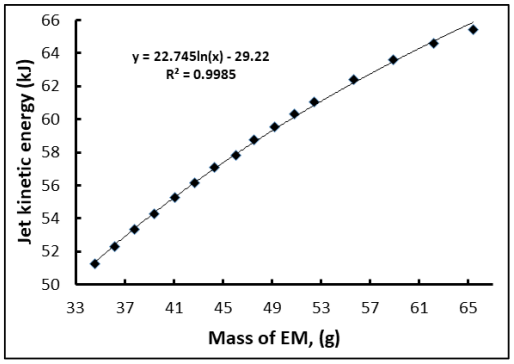

Figure 8. Predicted jet kinetic energy with the mass of EM.

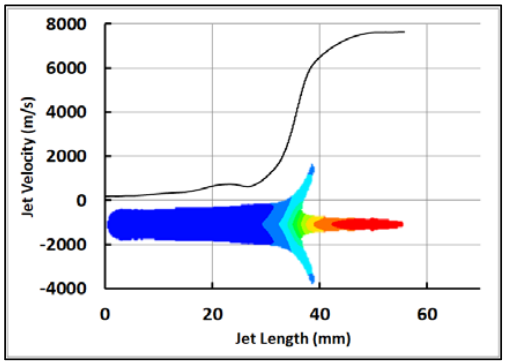

Figure 9. Profile of the jet velocity-length for a perforator charge with mass of EM of 42.6g.

4.4. Jet breakup time results

For each perforator charge, the proposed formula by Hirsch [21] is used for determining the jet breakup time for each jet element t_{bi}. Then, the average breakup time of jet t_b is equal to the sum of the breakup times of the jet elements divided by their number. The breakup time of jet element is calculated by equation (7) as:

$$t_{bi} = \frac{2r}{V_{PL}} \tag{7}$$

where V_{PL} is the characteristic plastic velocity or the velocity difference between successive jet elements and r is the initial radius of jet element when the jet is just formed, which can be predicted by equation (8);

$$r = \sqrt{2R\,T_L}\sin\left(\frac{\beta}{2}\right) \tag{8}$$

where R is the radius of jet element from the liner axis, T_L is the liner wall thickness and β is the collapse angle of the jet element. The plastic velocity V_{PL} and the ratio of (T_L/CD) values are correlated for copper material according to Hirsch [22] as:

$$\frac{1}{V_{PL}} = 13.886 - 101.149\left(\frac{T_L}{C_D}\right). \tag{9}$$

The results of the calculated jet break up time for every perforator charge are listed in table 6, whereas the effect of the mass of EM on the average jet break up time is shown in figure 10.

Table 6. The calculated average break up time of jet formed from each perforator charge.

(a)

Trial design.	CD (mm)	Mass of EM, (g)	T_L, (mm)	t_b (μs)
A	33.0	34.57	1.1	24.55
B		36.20		24.75
C		37.82		24.95
D		39.44		25.13
E		41.07		25.30
F		42.69		25.47
G		44.31		25.63
H		46.08		25.78

(b)

Trial design.	CD (mm)	Mass of EM, (g)	T_L (mm)	t_b (μs)
I	33.0	47.56	1.1	25.93
J		49.18		26.06
K		50.81		26.20
L		52.43		26.33
M		55.67		26.56
N		58.92		26.79
O		62.16		27.00
p		65.41		27.20

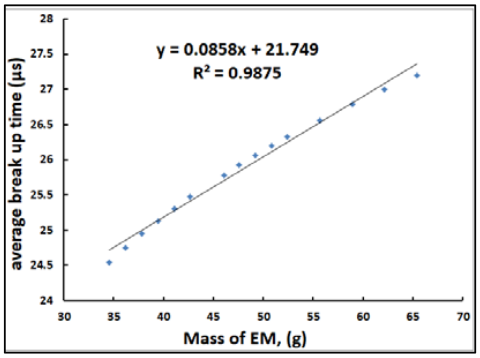

Figure 10. The effect of mass of EM on the average break up time**.**

4.5. Jet penetration results

In the present work, the jet penetration depth formed from each perforator charge into 1006 steel target is predicted using two algorithms of Autodyn-2D hydrocode; they are jetting analysis and jet penetration algorithms, respectively. For each perforator charge, the jetting analysis results are used for determining the effective length of jet prior to impact into steel target which is equivalent to the distance between the point of virtual origin and target surface Z_o. Then, these data are used to predict the penetration depth of jet into metallic target by applying the explicit formulae based on Allison and Vitali's theory [19] when the breakup time is estimated. It was found that the explicit formula used for predicting each jet penetration depth of the perforator charges loaded with the mass of EM ranged from 34.57 up to 65.41 g into steel target is:

$$P = \frac{(1+\gamma)\left(V_{tip}\,t_b\right)^{\frac{1}{(1+\gamma)}}\,Z_o^{\frac{\gamma}{1+\gamma}} - V_{min}t_b}{\gamma} - Z_o\,. \tag{10}$$

when

$$V_{tip}t_b\left(\frac{V_{min}}{V_{tip}}\right)^{\frac{1}{\gamma}} \leq Z_o < V_{tip}t_b\,, \tag{11}$$

where P is the penetration depth into the target, γ is the ratio of the square root of target density to jet density, V_{tip} is the jet tip velocity, t_b the average breakup time, V_{min} is the cut-off velocity and Z_o is the effective length of jet (*i.e.* the stand-off distance plus the distance from the virtual origin to the liner base). This effective length is bounded by Eq(11):

In order to locate the virtual origin point and calculate the effective jet length, the back projection method [20] is used as shown in figure 11 for perforator charge E, in which the jet formation algorithm is employed for further back projection to locate the virtual origin point using two points "the stagnation point and the jet tip element". Similarly, the same method has been implemented with the entire masses of EM and relevant stand-off distances to calculate the jet penetration analytically. The jet formation algorithm was used to obtain the jet contours, the stretching shape, and the time and axial distances for both the jet tip and the stagnation points; respectively.

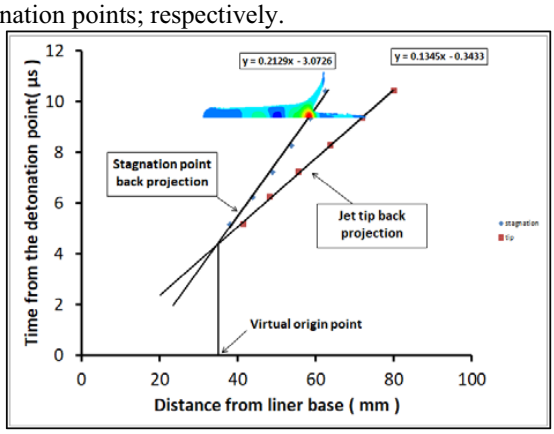

Figure 11. The back projection method used to determine the location of the virtual origin point and effective jet length for the perforator charge E.

In addition to the analytical formula of the penetration depth, further numerical work based on Lagrange-Lagrange interaction in jet penetration algorithm of Autodyn-2D hydrocode is performed. In such algorithm, the remapped jet is allowed to penetrate into the steel target to identify the penetration depth when the jet is totally consumed on the crater walls or when the jet element velocity fall below the critical cutoff velocity. The final numerical penetration of the tested charges is shown in figure 12 for these charges with the details of crater profile. For the first impression, the EM mass of 41.07g with relevant standoff distance of 22.6mm gives the best penetration depth into steel target compared with the other designed perforator charges.

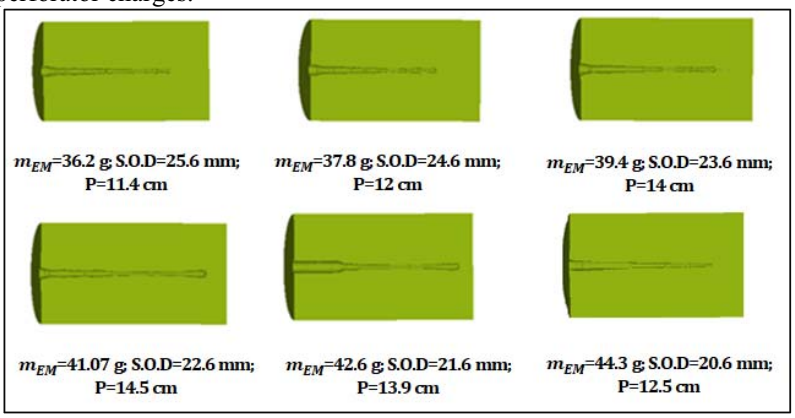

Figure 12. Predicted crater profiles inside the steel target using different masses of EM.

Further confirmation of the predicted results is the penetration measurements due to the static exploding of the constructed perforator charges with different masses of EM and relevant standoff distance on steel target shown in figure 13. The entire penetration results; analytical, experimental and the numerical are listed in table 7 with the relevant calculated error percent. Results show that there is great dependence on both the used mass of EM and the relevant standoff distance. The measured penetration depth increases from 11.0cm to 13.7cm when the mass of EM increases from 36 to 41 g and the relevant standoff distances decreases from 25.6 to 22.6mm. Experimental tests show the increase in penetration from 11cm relevant to 36 g EM to 13.7cm relevant to 41g and 22.6mm standoff distance. Beyond this value, the penetration decreases again due to the limited standoff distance although the mass of EM increases. This fact is confirmed by both the numerical and the analytical approach results listed in the same table.

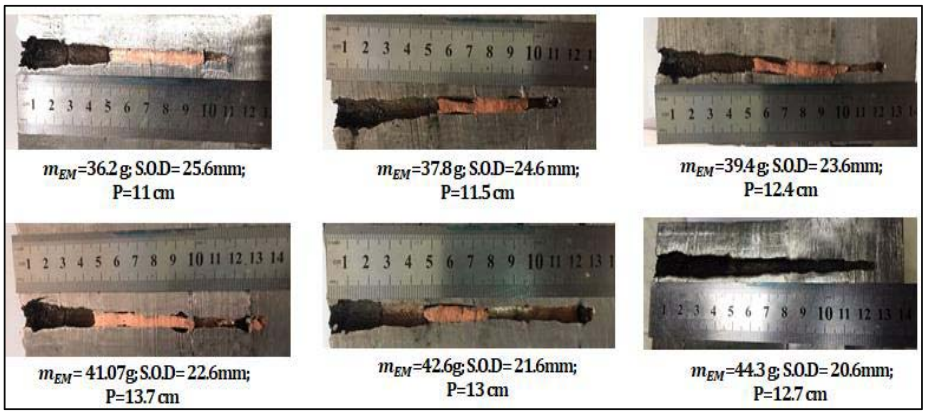

Figure 13. Measured penetration depth for perforator charges with different masses of EM.

Table 7. Jetting analysis results obtained using Autodyn hydrocode, and the analytical, numerical and measured penetration depths, respectively.

Desig.	Mass of EM (g)	Tip vel., V_{tip} (m/s)	Cut-off vel. V_{min} (m/s)	Eff. Length of jet, Z_o (mm)	Ave. break. time, t_b (μs)	γ (-)	Penetration depth, P (cm)			Abs. error[a]. ΔP_1 (%)	Abs. Error[b]. ΔP_2 (%)
							Eq. (10)	Autod.	Meas.		
B	36.20	8639	1800	53.87	21.37	0.934	12.57	11.4	11.0	14.3	3.64
C	37.82	8667	1650	53.30	21.54	0.934	13.00	12.0	11.5	13.04	4.35
D	39.44	8698	1235	52.72	21.68	0.934	14.15	14.0	12.4	14.1	12.9
E	41.07	8754	1115	52.19	21.82	0.934	14.54	14.5	13.7	6.13	5.84
F	42.69	8795	1233	52.00	21.93	0.934	14.32	13.9	13.0	10.15	6.92
G	44.31	8842	1378	51.31	22.03	0.934	13.95	12.5	12.7	9.84	1.57

[a]: Error $\Delta P_1(\%) = 100x(P_{meas} - P_{Eqn.(10)})/ P_{meas}$. [b]: Error $\Delta P_2 (\%) = 100x(P_{meas} - P_{Autodyn})/ P_{meas}$.

The different approaches used in the present work give different values within the entire research work with maximum error between the numerical penetration depth and the corresponding measurement about 12.9%, in comparison to 14.3% as a maximum error between the measured and the corresponding prediction of Eqn. (10) as shown in Figure 14. Moreover, the studied approaches prove a significant finding; there is an optimum value of the used mass of EM to be loaded within the selected perforator charge, at which the penetration depth is maximum at the maintained standoff distance. Beyond this value the penetration decreases again due to the very short standoff distance at which the jet does not become fully generated however, more masses of EM are loaded in perforator charges.

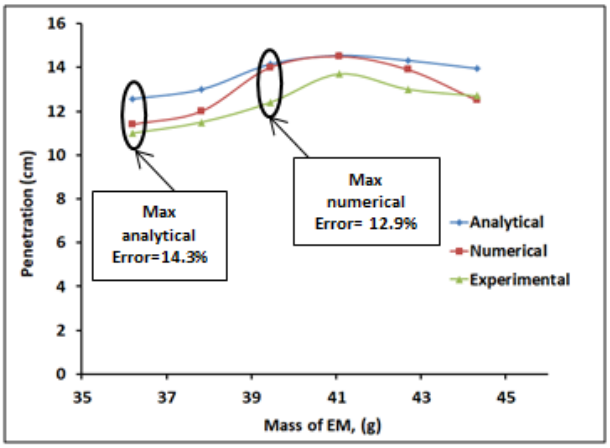

Figure 14. Analytical, numerical and experimental penetration dependence on the mass of EM.

5. Conclusions

The main conclusions of the present work are:

- 16 perforator charges with different masses of EM and relevant stand-off distances have been simulated into Autodyn-2D hydrocode to investigate their penetration performance into 1006 steel target and to determine the best design that may be selected according to jet energy characteristics.
- The jetting analysis results predict that the increase in the mass of EM increases the jet collapse, flow and tip velocities, as well as the jet mass and its ratio to the liner mass in percent.
- The average breakup time of the formed jet from perforator charges increases in quasi-linear manner with the mass of EM.
- The jet penetration depth into 1006 steel target is predicted for only 6 perforated charges using two different algorithms of Autodyn-2D hydrocode. Results of jetting analysis algorithm are used to feed the analytical formulae with the data for calculating the jet penetration depth into 1006 steel target via virtual origin point model developed in Ref. [19] whereas; the jet penetration algorithm predicts the jet penetration into steel target directly.
- The ballistic test results of perforator charges show that the measured depth increases from 11.0cm to 13.7cm when the mass of EM increases from 36 to 41 g and the relevant standoff distances decreases from 25.6 to 22.6mm. Beyond this value, the penetration decreases again due to the limited decreases in standoff distances however, the mass of EM increases.
- The maximum absolute errors between the measured and the corresponding predicted penetration depths using equation (10) and Autodyn-2D hydrocode are found to be 14.1% and 12.9%, respectively.
- The different studied approaches predict an optimum value of the used mass of EM to be loaded within the selected perforator charge, at which the penetration depth is maximum at the maintained standoff distance.

6. References

[1] Walters W P and Zukas J 1989 Fundamentals of Shaped Charges *Wiley-Interscience, NY, USA*
[2] Schwartz A Kumar M and Lassila D 2004 Analysis of Intergranular Impurity Concentration and the Effects on the Ductility of Copper-Shaped Charge Jets. *J. of Metallurgical and Materials Transactions A 35 9 2567-573.*
[3] Zhao Z Liu J Guo W Li S. and Wang G 2016 Effect of Zn and Ni Added in W–Cu Alloy on Penetration Performance and Penetration Mechanism of Shaped Charge Liner. *I J Refractory Metals Hard Mater 54 90–7.*
[4] Fu J P Chen Z G Hou X C Li S Q Li S C and Wang J W 2013 Simulation and Experimental Investigation of Jetting Penetrator Charge At Large Stand-off Distance. *Defence Technology 9 91–7.*
[5] Hazell P J 2016 Armour: materials, theory and design. *Florida: Taylor & Francis Group.*

[6] Held M F 1988 Penetration Cutoff Velocities of Shaped Charge Jets. *Propellants, Explosives, Pyrotechnics 13 4 111-19.*
[7] Dehestani P Fathi A R and Daniali H M 2019 Numerical Study of the Stand-off Distance and Liner Thickness Effect on the Penetration Depth Efficiency of Shaped Charge Process *Proceedings of the Institution of Mechanical Engineers, Part C: J. of Mechanical Engineering Science* 3 977-98.
[8] Ngo T S Beer S Konečný P and Van Bien V 2019 Simulation Study of Shaped Charge Collapse Process and Optimal Standoff Determination. *International Conference on Military Technologies (ICMT) IEEE 1-5.*
[9] El-Sayed E E Elshenawy T A Shaker M A and Riad A M 2022 Influence of Different Shaped Charge Parameters on Jet Penetration into Metallic Target. *In: Journal of Physics: Conference Series. IOP Publishing, p. 012016.*
[10] Zaki S Uddin E Rashid B Mubashar A and Shah S R 2019 Effect of liner material and explosive type on penetration effectiveness of shaped charge. *Proceedings of the Institution of Mechanical Engineers, Part L: Journal of Materials: Design and Applications 233 7 1375-383.*
[11] Doig A 2020 Military Metallurgy. *CRC Press*.
[12] Pugh E M Eichelberger R J and Rostoker N. 1952 Theory of Jet Formation by Charges with Lined Conical Cavities. *Journal of Applied Physics 23 5 p. 532.*
[13] Malcolm S (Edditor) 1997 Autodyn Theory Manual, R. 3.0, *Century Dynamics: U S A.*
[14] Berg V S and Preece D S 2004 Shaped Charge Induced Concrete Damage Predictions Using RHT Constitutive Modeling. *Journal of International society of explosives engineers 2.*
[15] Tarver C M Tao W C and Lee C G 1996 Sideways Plate Push Test for Detonating Solid Explosives. *Propellants, Explosives, Pyrotechnics, 21 5 p. 238*.
[16] Johnson and Cook W 1983 A Constitutive Model and Data for Metals Subjected to Large Strains, High Strain Rates and High Temperatures. *Proceedings of the 7th Int. Symposium on Ballistics.*
[17] API, Recommended Practice 19B for Evaluation of Well Perforators, *First Edition, November 2001.*
[18] Malcolm S (Edditor) 1997 Autodyn User Manual, R. 3.0, *Century Dynamics: U S A.*
[19] Allison F E and Vitali R 1963 A New Method of Computing Penetration Variables for Shaped Charge Jets. *Aberdeen Proving Ground, Ballistic Research Lab., Report No 1184, Maryland,*
[20] Elshenawy T Elbeih A Klapötke T M 2018 A Numerical Method for the Determination of the Virtual Origin Point of Shaped Charge Jets Instead of Using Flash X-ray Radiography. *J. Energ. Mater. 36 2: 127-40.*
[21] Hirsch E 1979 A Formula for the Shaped Charge Jet Breakup-Time. *Propellants, Explosives, Pyrotechnics 4 5 pp. 89-94.*
[22] Hirsch E 2006 Scaling of the Shaped Charge Jet Break Up Time. *Propellants, Explosives, Pyrotechnics, 31 3 pp. 230-33.*